Zero-Crossings of a Wavelet Transform

Stephane Mallat

Abstract—**Sharp variation points are among the most meaningful features for characterizing transient signals. For a particular class of wavelets, the zero-crossings of a wavelet transform provide the locations of the signal sharp variation points at different scales. The completeness and stability of a signal representation based on zero-crossings of a wavelet transform at the scales 2^j, for integer j are studied. An alternative projection algorithm is described. It reconstructs a signal from a zero-crossing representation which is stabilized. The reconstruction algorithm has a fast convergence and each iteration requires $O(N \log^2(N))$ computations for a signal of N samples. The zero-crossings of a wavelet transform define a representation which is well adapted for solving pattern recognition problems. As an example, the implementation and results of a coarse-to-fine stereo-matching algorithm are described.**

Index Terms—**Multiscale, pattern matching, signal representation, wavelet transform, zero-crossings.**

I. Introduction

An important problem in signal processing is to define a representation that is well adapted for extracting the information content of signals. The sharp variations of a signal amplitude are generally among the most meaningful features. For example, the discontinuities of an image intensity provide the contours of the different objects. When the signal includes important structures that belong to different scales, it is often helpful to reorganize the signal information into a set of "detail components" of varying size [17]. Marr and Hildreth [14] have shown that one can obtain the position of multiscale sharp variations points from the zero-crossings of the signal convolved with the Laplacian of a Gaussian. This edge detection procedure has been used in many pattern recognition applications [4]. An important practical and theoretical issue is to understand whether the multiscale edges carry all the information of the original signal. Indeed, for pattern recognition applications, we do not want to remove some important components of the signal, when representing it with multiscale zero-crossings. Completeness by itself is not sufficient as for most applications the representation must also be stable. This means that a small perturbation of the representation should correspond to a small modification of the original signal. While reviewing some previous work, we shall see that the positions of multiscale zero-crossings may provide a complete representation under certain restrictive assumptions but such a representation is not stable. We show that one can stabilize a zero-crossing representation by adding a complement of information that measures the "size" of the structure between two consecutive zero-crossings. This new signal representation is based on the wavelet transform reformalization of multiscale decompositions. We introduce the most important results of the wavelet theory in order to study the properties of multiscale zero-crossings. The central result of this article is an algorithm that reconstructs one-dimensional signals from a stabilized zero-crossing representation. This algorithm iterates on a nonexpansive projector on a convex set and an orthogonal projector on a Hilbert space, hence the convergence is guaranteed. The numerical results show that the reconstruction is independent from the choice of the initial point at the beginning of the iteration but this has not been proven mathematically. The convergence is fast and each iteration requires $O(N \log^2(N))$ computations, for a signal of N samples.

In order to illustrate the application of this new zero-crossing representation to pattern recognition, we describe the results of a stereo-matching algorithm. The stereo matching problem consists of finding a point by point correspondence between two one-dimensional signals that are shifted from one another and have some local distortions. In image processing, we must solve such a correspondence problem when trying to recover a depth information from a pair of stereo images. We introduce a simple distance based on our multiscale zero-crossing representation and derive a coarse to fine matching algorithm to compute the stereo correspondence. Matching results on two epipolar lines of real images are given.

A. Notation

$\boldsymbol{Z}$ denotes the set of integers. $\boldsymbol{L}^2$ denotes the Hilbert space of measurable, square-integrable one-dimensional functions. For $f(x) \in \boldsymbol{L}^2$ and $g(x) \in \boldsymbol{L}^2$, the inner product of $f(x)$ with $g(x)$ is

$$\langle g(x), f(x) \rangle = \int_{-\infty}^{+\infty} g(x) f(x)\, dx.$$

Manuscript received August 26, 1988; revised October 15, 1990. This work was supported by the National Science Foundation Grant IRI-890331 and Air Force Grant AFOSR-90-0040.

The author is with the Computer Science Department, Courant Institute of Mathematical Sciences, New York University, New York, NY 10012.

IEEE Log Number 9144606.

0018-9448/91/0700-1019$01.00 ©1991 IEEE

The norm of $f(x) \in L^2$ is given by

$$\|f\|^2 = \int_{-\infty}^{+\infty} |f(x)|^2 \, dx.$$

We also denote by $l^2(L^2)$ the Hilbert space of all sequences of functions $(g_j(x))_{j \in Z}$, such that for all $j \in Z$, $g_j(x) \in L^2$ and

$$\sum_{j=-\infty}^{+\infty} \|g_j(x)\|^2 < +\infty.$$

This infinite sum is the norm of the sequence $(g_j(x))_{j \in Z}$ in $l^2(L^2)$.

We denote the convolution of two functions $f(x) \in L^2$ and $g(x) \in L^2$ by

$$f * g(x) = \int_{-\infty}^{+\infty} f(u) g(x-u) \, du.$$

The Fourier transform of $f(x) \in L^2$ is written $\hat{f}(\omega)$ and is defined by

$$\hat{f}(\omega) = \int_{-\infty}^{+\infty} f(x) e^{i\omega x} \, dx.$$

II. Properties of the Wavelet Transform

The wavelet transform is a linear operation that decomposes a signal into components that appear at different scales. This transform is based on the convolution of the signal with a dilated filter. Such a decomposition has been studied in signal processing [19] and computer vision [20] but has recently been reformalized in mathematics. For a thorough presentation, the reader is referred to general reviews [2], [12] and an advanced functional analysis book of Meyer [16]. A wavelet is a function $\psi(x) \in L^2$ such that

$$\int_{-\infty}^{+\infty} \psi(x) \, dx = 0.$$

Let us denote by $\psi_s(x)$ the dilation of $\psi(x)$ by a factor s:

$$\psi_s(x) = \frac{1}{s} \psi\left(\frac{x}{s}\right). \tag{1}$$

The wavelet transform of a function $f(x)$ at the scale s and position x is given by the convolution product

$$W_s f(x) = f * \psi_s(x). \tag{2}$$

Morlet and Grossmann [5] have shown that the wavelet transform satisfies an energy conservation equation and that $f(x)$ can be reconstructed from its wavelet transform. When the scale s decreases, the support of $\psi_s(x)$ decreases so the wavelet transform $W_s f(x)$ is sensitive to finer details. The scale s characterizes the size and regularity of the signal features extracted by the wavelet transform.

The wavelet transform depends on two parameters s and x that vary continuously over the set of real numbers. For practical applications these parameters must be discretized. For a particular class of wavelets, the scale parameter can be sampled along the dyadic sequence $(2^j)_{j \in Z}$, without modifying the overall properties of the transform. The principles of such a dyadic scale decomposition was studied in mathematics by Littlewood and Paley in the 1930's. The wavelet transform at the scale 2^j is given by

$$W_{2^j} f(x) = f * \psi_{2^j}(x). \tag{3}$$

At each scale 2^j, the function $W_{2^j} f(x)$ is continuous since it is equal to the convolution of two functions in L^2. The Fourier transform of $W_{2^j} f(x)$ is

$$\hat{W} f_{2^j}(\omega) = \hat{f}(\omega) \hat{\psi}(2^j \omega). \tag{4}$$

By imposing that

$$\sum_{j=-\infty}^{+\infty} |\hat{\psi}(2^j \omega)|^2 = 1, \tag{5}$$

we insure that the whole frequency axis is covered by a dilation of $\hat{\psi}(\omega)$ by the scales factors $(2^j)_{j \in Z}$. Any wavelet satisfying equation (5) is called a *dyadic wavelet*. We also call *dyadic wavelet transform* the sequence of functions

$$(W_{2^j} f(x))_{j \in Z}. \tag{6}$$

We denote by W the dyadic wavelet operator defined by $Wf = (W_{2^j} f(x))_{j \in Z}$.

From (4) and (5) and by applying the Parseval theorem, we obtain an energy conservations equation

$$\|f\|^2 = \sum_{j=-\infty}^{+\infty} \|W_{2^j} f(x)\|^2. \tag{7}$$

Let $\tilde{\psi}_{2^j}(x) = \psi_{2^j}(-x)$. The function $f(x)$ can be reconstructed from its dyadic wavelet transform:

$$f(x) = \sum_{j=-\infty}^{+\infty} W_{2^j} f * \tilde{\psi}_{2^j}(x). \tag{8}$$

This equation is proved by computing its Fourier transform and inserting (4) and (5).

Let V be the space of the dyadic wavelet transforms $(W_{2^j} f(x))_{j \in Z}$, for all functions $f(x) \in L^2$. Let us denote by $l^2(L^2)$ the Hilbert space of all sequences of functions $(g_j(x))_{j \in Z}$, such that

$$g_j(x) \in L^2 \quad \text{and} \quad \sum_{j=-\infty}^{+\infty} \|g_j(x)\|^2 < +\infty.$$

Equation (7) proves that V is a subspace of $l^2(L^2)$. We denote by W^{-1} the operator from $l^2(L^2)$ to L^2 defined by

$$W^{-1}(g_j(x))_{j \in Z} = \sum_{j=-\infty}^{+\infty} g_j * \tilde{\psi}_{2^j}(x). \tag{9}$$

The reconstruction formula (8) shows that the restriction of W^{-1} to the wavelet space V is the inverse of the dyadic wavelet transform operator W.

Any sequence of functions $(g_j(x))_{j \in Z} \in l^2(L^2)$ is not *a priori* the dyadic wavelet transform of some function $f(x) \in L^2$. Indeed, if there exists a function $f(x) \in L^2$ such that $(g_j(x))_{j \in Z} = Wf$, then clearly we should have

$$W\left(W^{-1}(g_j(x))_{j \in Z}\right) = (g_j(x))_{j \in Z}. \tag{10}$$

If we replace the operators W and W^{-1} by their expres-

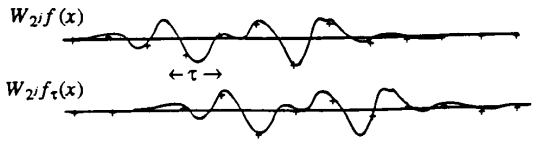

Fig. 1. When $f(x)$ is translated by τ, its wavelet transform $W_{2^j}f(x)$ is also translated. However, samples of $W_{2^j}f(x)$ and $W_{2^j}f_\tau(x)$ (given by the crosses) are not translated from one-another if the translation τ is not proportional to the sampling interval $r2^j$.

sion given in (3) and (9), we obtain:

$$\forall j \in \mathbf{Z}, \qquad \sum_{l=-\infty}^{+\infty} g_l * K_{l,j}(x) = g_j(x),$$

with

$$K_{l,j}(x) = \tilde{\psi}_{2^l} * \psi_{2^j}(x). \tag{11}$$

The sequence $(g_j(x))_{j\in\mathbf{Z}}$ is a dyadic wavelet transform if and only if (11) holds. These equations are called reproducing kernel equations. They express the correlation between the functions $W_{2^j}f(x)$ of a dyadic wavelet transform. The operator

$$\boldsymbol{P}_V = \boldsymbol{W} \circ \boldsymbol{W}^{-1} \tag{12}$$

is a projector from $l^2(\boldsymbol{L}^2)$ on the V space. Indeed, one can easily prove that any sequence of functions

$$\left(g_j(x)\right)_{j\in\mathbf{Z}} \in l^2(\boldsymbol{L}^2)$$

satisfies $\boldsymbol{P}_V(g_j(x))_{j\in\mathbf{Z}} \in V$, and we saw that any element of V is invariant under the action of this operator. One can also prove that the projector $\boldsymbol{P}_V$ is orthogonal in $l^2(\boldsymbol{L}^2)$ because it is derived from a reproducing kernel equation. This projector is important for the purpose of this paper.

For digital processing applications, the spatial parameter x of the functions $W_{2^j}f(x)$ must also be discretized. The classical approach consists in sampling each function $W_{2^j}f(x)$ with a sampling interval $r2^j$. If r is small enough, Daubechies [3] has proved that $f(x)$ can be recovered from the set of samples $(W^jf(n/r2^j))_{(n,j)\in\mathbf{Z}^2}$. The fundamental drawback of this sampling procedure is that it is perturbated by any translation. Let $f(x) \in \boldsymbol{L}^2$ and $f_\tau(x) = f(x-\tau)$ be a translation of $f(x)$ by τ. Since the wavelet transform is defined with a convolution product, we can derive that

$$W_{2^j}f_\tau(x) = W_{2^j}f(x-\tau). \tag{13}$$

However, the sampling of $W_{2^j}f_\tau(x)$ does not correspond to a translation of the sampling of $W_{2^j}f(x)$ unless $\tau = kr2^j$, $k \in \mathbf{Z}$ (see Fig. 1).

The uniform sampling of a wavelet transform is difficult to use for pattern recognition since it does not define signal descriptors that translate when the signal is translated. Indeed, the wavelet coefficients of a particular pattern are modified when the position of this pattern is changed. On the contrary, it is clear that the position of the zero-crossings of a dyadic wavelet transform are translated when the signal $f(x)$ is translated.

Let us now study in more detail the properties of the wavelet transform zero-crossings. We call smoothing function the impulse response of a low-pass filter. The convolution of a function $f(x)$ with a smoothing function attenuates part of its high frequencies without modifying the lowest frequencies and hence smooths $f(x)$. Let us show that if the wavelet is the second derivative of a smoothing function, the zero-crossings of a wavelet transform indicate the location of the signal sharper variation points. Let $\theta(x)$ be a smoothing function, and

$$\psi(x) = \frac{d^2\theta(x)}{dx^2}. \tag{14}$$

We denote $\theta_s(x) = (1/s)\theta(x/s)$ the dilaton of $\theta(x)$ by a factor s. Since

$$W_sf(x) = f * \psi_s(x), \tag{15}$$

we derive that

$$W_sf(x) = f * \left(s^2 \frac{d^2\theta_s}{dx^2}\right)(x) = s^2 \frac{d^2}{dx^2}(f * \theta_s)(x). \tag{16}$$

Hence, $W_sf(x)$ is proportional to the second derivative of $f(x)$ smoothed by $\theta_s(x)$. The zero-crossings of $W_sf(x)$ correspond to the inflection points of $f * \theta_s(x)$. When the smoothing function $\theta(x)$ is a Gaussian, detecting the zero-crossings of a wavelet transform is equivalent to a Marr–Hildreth edge detector [14].

III. Review of Completeness and Stability Results from Zero-Crossings

A fundamental issue is to understand whether the zero-crossings define a complete and stable representation of the original signal. We briefly review some previous results on this problem. The most classical result concerning the characterization of a signal from its zero-crossings is due to Logan [9]. We describe in some detail Logan's theorem because it provides a good understanding of the mathematical issues. Let $f(x) \in \boldsymbol{L}^2$ and let us suppose that its Fourier transform has a support included in one octave intervals. Logan theorem [9] proves that if $f(x)$ does not share any zero-crossings with its Hilbert transform, then it is uniquely characterized by its zero-crossings. Let us give an intuitive justification of this result. We know that there exists ω_0 such that the Fourier transform of $f(x)$ has a support included in the intervals $[-2\omega_0, -\omega_0] \cup [\omega_0, 2\omega_0]$. The Nyquist theorem proves that such a signal is characterized by a uniform sampling at the rate ω_0/π. One can also prove that this signal changes sign approximatively as frequently as the function $\sin(\omega_0 x)$. The number of zero-crossings is therefore of the same order than the number of values needed to characterize the signal with a uniform sampling. Of course, the zero-crossing problem is different since zero-crossings are not uniformly distributed, but one can see that qualitatively the same amount of information is available. To prove this theorem, Logan makes an analytic extension of the signal and uses standard properties of zeros of ana-

lytic functions. The zero-crossing characterization as explained by Logan is not stable: "the problem of actually recovering (the signal) from its sign changes appears to be very difficult and impractical."

Let us now explain how Logan's theorem can be integrated in the wavelet model. Let $\psi(x)$ be the function equal to the impulse response of a perfect bandpass filter of one octave. Its Fourier transform is given by

$$\hat{\psi}(\omega) = \begin{cases} 1, & \text{if } \pi \le |\omega| \le 2\pi, \\ 0, & \text{otherwise.} \end{cases} \tag{17}$$

The function $\psi(x)$ clearly satisfies (5) and is therefore a dyadic wavelet. Let $f(x) \in \boldsymbol{L}^2$; the Fourier transform of $W_{2^j} f(x)$ is given by $\hat{W}_{2^j} f(\omega) = \hat{f}(\omega)\hat{\psi}(2^j\omega)$. The support of $\hat{W}_{2^j} f(\omega)$ is thus included in the one octave intervals $[-2^{-j+1}\pi, -2^{-j}\pi] \cup [2^{-j}\pi, 2^{-j+1}\pi]$. From Logan's theorem we derive that each function $W_{2^j} f(x)$ is characterized by its zero-crossings. Since we can reconstruct $f(x)$ from $(W_{2^j} f(x))_{j \in Z}$, the original function $f(x)$ is also characterized by the zero-crossings of all the functions $(W_{2^j} f(x))_{j \in Z}$. This characterization is however not stable as previously explained.

Although Logan's theorem is an important result, we want now to emphasize the reason why it cannot be used for the type of wavelets we are interested in. We need a wavelet equal to the second derivative of some smoothing function so that zero-crossings indicate the position of the signal shaper variation points. If $\psi(x) = (d^2\theta(x))/dx^2$, then its Fourier transform can be written $\hat{\psi}(\omega) = -\omega^2\hat{\theta}(\omega)$. Since $\theta(x)$ is the impulse response of a low-pass filter, it satisfies $\hat{\theta}(0) \neq 0$ so $\hat{\psi}(\omega)$ has a zero of order two at $\omega = 0$. Similarly, one can show that a wavelet is the nth-order derivative of some smoothing function only if its Fourier transform $\hat{\psi}(\omega)$ has a zero of order n at $\omega = 0$. The Logan wavelet $\psi(x)$ given in (17) cannot be written as a finite-order derivative of some smoothing function since its Fourier transform has an infinite-order zero in $\omega = 0$. Hence, the zero-crossings of the wavelet transform $W_{2^j} f(x)$ can not be interpreted as any particularly interesting features of $f(x)$. In fact, there are too much zero-crossings since $W_{2^j} f(x)$ changes sign in almost all intervals of length 2^j, for any function $f(x)$. Logan as well as other researchers who extended this result, use the band-limited properties of the signal for computing its analytic extension. All these proofs do not provide any stability result since they are based on nonstable characterization of analytical functions [1], [18], [23]. The reader is referred to a review by Hummel and Moniot for more details [7].

Many studies have also described the properties of zero-crossings of functions convolved with the Laplacian of a Gaussian. This convolution is equivalent to the wavelet transform built with a wavelet $\psi(x)$ equal to the Laplacian of a Gaussian. Such a wavelet transform can be interpreted as the result of a heat diffusion process [8]. Indeed, the Gaussian is the Green function of the heat diffusion equation. Let $t = s^2$ be the diffusion time, one can show that the wavelet transform $W_s f(x)$ built with the Laplacian of a Gaussian satisfies the heat differential equation

$$\frac{\partial W_s f(x)}{\partial t} = \frac{\partial^2 W_s f(x)}{\partial x^2}. \tag{18}$$

The wavelet transform $W_s f(x)$ is therefore equal to a heat distribution after a diffusion time $t = s^2$ with an initial heat distribution at $t = 0$ equal to $\Delta f(x)$ (the Lapalcian is taken in the sense of distributions). By using the maximum principle, several authors have proved interesting properties of the propagation of zero-crossings across scales [6], [8], [22]. Hummel and Moniot as well as Yuille and Poggio have also proven that the position of the zero-crossings of $W_s f(x)$ give a complete characterization of any function $f(x)$ equal to a polynomial of arbitrary high order [6]. If $f(x)$ is a polynomial then the function $F(s, x) = W_s f(x)$ is a polynomial in $(s, x) \in \boldsymbol{R}^+ \times \boldsymbol{R}$, so the problem is reduced to the characterization of a polynomial from the locus of its real roots. The proof is based on an analytic continuation result so the stability of the reconstruction is unlikely [7]. The polynomial assumption can not be extended by a density argument because of this instability. Numerical results [7] show that one can build signals which are quite different although the zero-crossings of their wavelet transform are very close. It is difficult to make a formal proof of the instability of a zero-crossing representation because the notion of instability is not well defined. A representation is said to be unstable if a small perturbation of the representation may correspond to an arbitrary large perturbation of the original function. In order to measure the modification of the representation, we must define a metric on zero-crossings. The problem is that there is no satisfactory metric based only on the position of multiscale zero-crossings.

In order to stabilize the reconstruction of a function from its zero-crossings, Hummel records the gradient of the wavelet transform along each zero-crossing. Hummel and Moniot [6] have implemented an algorithm for reconstructing the signal from the zero-crossings and gradient values. The algorithm is essentially based on the differential equation (18) that gives the evolutionary properties of $W_s f(x)$ when the scale s and the abscissa x vary. The zero-crossing information of $W_s f(x)$ is computed for s varying along a uniform discrete sequence with a scale interval Δs: $(j \cdot \Delta s)_{j \in Z}$. The convergence of the reconstruction algorithm is not proven but the numerical experiments show that it converges slowly. This reconstruction procedure is computationally intensive. The differential equation approach is only valid for a wavelet equal to the Laplacian of a Gaussian and it is required to record the zero-crossing information on a dense sequence of scales. In the following sections, we show that the reproducing kernel equation of a wavelet transform provides a general procedure to reconstruct a function from a stabilized zero-crossing representation, for any type of wavelet. This approach enables us to record the zero-crossing information only along the sparse sequence of scales $(2^j)_{j \in Z}$, and

the corresponding reconstruction algorithm has a fast convergence.

IV. Stabilized Zero-Crossing Representation

Instead of considering the zero-crossings of a wavelet transform on a continuum of scales s, we restrict ourselves to dyadic scales $(2^j)_{j\in Z}$. In order to stabilize the zero-crossing representation, we also record the value of the wavelet transform integral between two zero-crossings. We compute an integral measure instead of a gradient value because it will then enables us to define a simple L^2 norm on the zero-crossing representation. This is particularly important for pattern recognition applications, as explained in Sections VIII and IX.

Let $f(x)\in L^2$ and $(W_{2^j}f(x))_{j\in Z}$ be its dyadic wavelet transform. For any pair of consecutive zero-crossings of $W_{2^j}f(x)$ whose abscissae are respectively (z_{n-1}, z_n), we record the value of the integral

$$e_n = \int_{z_{n-1}}^{z_n} W_{2^j}f(x)\,dx. \tag{19}$$

Equation (16) proves that

$$W_{2^j}f(x) = 2^{2j}\frac{d^2}{dx^2}(f*\theta_{2^j})(x). \tag{20}$$

Since z_{n-1} and z_n are two zero-crossings of $W_{2^j}f(x)$, these abscissa correspond to two consecutive extrema of $(d/dx)(f*\theta_{2^j})(x)$. Equations (19) and (20) yield

$$e_n = 2^{2j}\left(\frac{d}{dx}(f*\theta_{2^j})(z_n) - \frac{d}{dx}(f*\theta_{2^j})(z_{n-1})\right).$$

The integral e_n is proportional to the difference between two consecutive extrema of the derivative of $f(x)$ smoothed at the scale 2^j. This value gives an estimate of the size of the structure which is between the two "edges" located at z_{n-1} and z_n. If $W_{2^j}f(x)$ has a zero-crossing z_0 of minimum abscissa, then we consider that $-\infty$ is also a zero-crossing and we record the integral of $W_{2^j}f(x)$ between $-\infty$ and z_0. The equivalent is done if there exists a zero-crossing of maximum abscissa. In order to make sure that these integrals are finite, we suppose that $f(x)$ is absolutely integrable.

For any function $W_{2^j}f(x)$, the position of the zero-crossings $(z_n)_{n\in Z}$ and the integral values $(e_n)_{n\in Z}$, can be represented by a piece-wise constant function $Z_{2^j}f(x)$ defined by

$$Z_{2^j}f(x) = \frac{e_n}{z_n - z_{n-1}}, \qquad \text{for } x\in[z_{n-1}, z_n]. \tag{21}$$

In Appendix IV, we explain how to define the zero-crossings of any function in L^2. The function $Z_{2^j}f(x)$ has the same zero-crossing and integral values as $W_{2^j}f(x)$ (see Fig. 2). If there exists a zero-crossing z_0 of minimum abscissa, then between $-\infty$ and z_0, $Z_{2^j}f(x)$ is zero on an interval $]-\infty, z_0 - l]$ and is equal to a constant c on $]z_0 - l, z_0]$, where the values of the constants of l and c

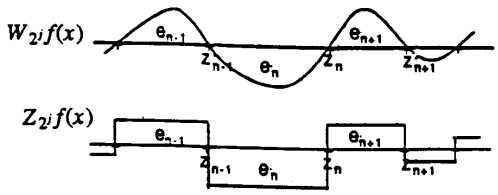

Fig. 2. Function $Z_{2^j}f(x)$ has the same zero-crossings and integral values as $W_{2^j}f(x)$ and is constant between two consecutive zero-crossings.

satisfy the constraints

$$\int_{-\infty}^{z_0} Z_{2^j}f(x)\,dx = \int_{-\infty}^{z_0} W_{2^j}f(x)\,dx, \tag{22}$$

$$\int_{-\infty}^{z_0} |Z_{2^j}f(x)|^2\,dx \le \int_{-\infty}^{z_0} |W_{2^j}f(x)|^2\,dx. \tag{23}$$

If there exists a zero-crossing of maximum abscissa, $Z_{2^j}f(x)$ is defined similarly between this zero-crossing and $+\infty$. Equation (23) enables us to prove in Appendix V that $\|Z_{2^j}f\| \le \|W_{2^j}f\|$ and that $(Z_{2^j}f(x))_{j\in Z}\in l^2(L^2)$. The sequence of piece-wise constant functions $Zf = (Z_{2^j}f(x))_{j\in Z}$ is called a *zero-crossing* representation of $f(x)$. Fig. 5(c) shows the zero-crossing representation of the signal in Fig. 5(a). As expected, the zero-crossings indicate the position of the sharper variation points of $f(x)$ smoothed at different scales.

V. Reconstruction from a Zero-Crossing Representation

Let us now study the reconstruction of a function from its zero-crossing representation. We reformalize the completeness problem within the wavelet framework and then derive an algorithm to perform the reconstruction. Let $f(x)\in L^2$ and $(W_{2^j}f(x))_{j\in Z}$ be its dyadic wavelet transform. Since $f(x)$ can be recovered from its dyadic wavelet transform, we first try to reconstruct $(W_{2^j}f(x))_{j\in Z}$ given the zero-crossings and integral values of each function $W_{2^j}f(x)$, $j\in Z$. Clearly, for any scale 2^j, there exists an infinite number of functions $g_j(x)$ that have the same zero-crossings and integral values as $W_{2^j}f(x)$. The piece-wise constant function $Z_{2^j}f(x)$ is an example. However, any such sequence of functions $(g_j(x))_{j\in Z}$ is not necessarily the dyadic wavelet transform of some function in L^2. Indeed, we saw in Section II that a dyadic wavelet transform must satisfy the reproducing kernel conditions (11). We thus have two types of information for reconstructing the functions $(W_{2^j}f(x))_{j\in Z}$. We know the zero-crossings and integral values of each function $W_{2^j}f(x)$ and we want to reconstruct a sequence of functions that satisfies the inner redundancy given by the reproducing kernel (11). Let us recall that $l^2(L^2)$ is the space of all sequence of functions $(g_j(x))_{j\in Z}$ such that $\sum_{-\infty}^{+\infty}\|g_j(x)\|^2 < +\infty$. The space of all dyadic wavelet transforms $(W_{2^j}f(x))_{j\in Z}$ is denoted V and is a subspace of $l^2(L^2)$. In order to express the conditions given by the zero-crossings of the wavelet transform of $f(x)$, we define the set Γ of all

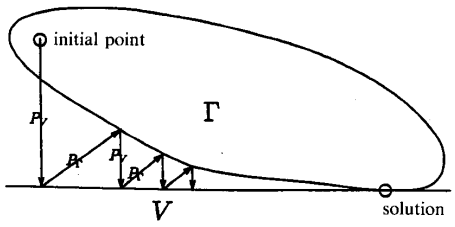

Fig. 3. To reconstruction of the wavelet transform of $f(x)$ from the zero-crossing representation, we iterate on a nonexpansive projector on Γ and an orthogonal projector on V, from an initial point $(g_j(x))_{j\in Z}$. Convex Γ expresses the constraints on the zero-crossing positions and the integral values. Hilbert space V is the space of all the dyadic wavelet transforms. Alternative projection is guaranteed to converge to the intersection of Γ and V.

sequences $(g_j(x))_{j\in Z}$ in $l^2(L^2)$ such that for all scales 2^j, $g_j(x)$ and $W_{2^j}f(x)$ have the same position of zero-crossings and the same integral value between all consecutive zero-crossings (z_{n-1}, z_n)

$$\int_{z_{n-1}}^{z_n} W_{2^j}f(x)\,dx = \int_{z_{n-1}}^{z_n} g_j(x)\,dx.$$

We explain in Appendix IV how to define the zero-crossing of a function in L^2 so that Γ is a closed convex set. The zero-crossing representation is complete if and only if there exists no dyadic wavelet transform different from $(W_{2^j}f(x))_{j\in Z}$ that has the same zero-crossings and integral values. In other words, the intersection of Γ with V must be reduced to one element

$$\Gamma \cap V = \{(W_{2^j}f(x))_{j\in Z}\}. \tag{24}$$

In order to verify numerically this assertion, we describe an algorithm that reconstructs the intersections of Γ with V.

A classical technique for recovering the intersection of a convex set with a linear space is to iterate on alternative projections on the convex and the linear space. Youla and Webb [21] wrote a review of the mathematical properties of these algorithms. For any $(g_j(x))_{j\in Z}$ in this Hilbert space, we can define a projection P_Γ on Γ that transforms $(g_j(x))_{j\in Z}$ into the sequence of functions $(h_j(x))_{j\in Z} \in \Gamma$ that is the closest to $(g_j(x))_{j\in Z}$. Since Γ is convex, the projection P_Γ is nonexpansive. The characterization of P_Γ is given in Appendix IV. Let P_V be the orthogonal projection on the space V, we saw in Section II that this operator can be written $P_V = W \circ W^{-1}$. Let $P = P_\Gamma \circ P_V$ be the composition of P_Γ and P_V. Clearly any element at the intersection of Γ and V is a fixed point of P. To compute such a fixed point, we iterate on the operator P as illustrated in Fig. 3. Let $P^{(n)}$ be the composition n times of the operator P. Since P_Γ is a nonexpansive projection on a closed convex and P_V is an orthogonal projection, one can prove [21] that for any initial sequence of functions $(g_j(x))_{j\in Z}$, when n tends to $+\infty$, $P^{(n)}(g_j(x))_{j\in Z}$ converges weakly to an element in $\Gamma \cap V$. This ensures that the iterative algorithm converges, but in order to prove that it reconstructs the dyadic wavelet transform of $f(x)$, for all initial sequences $(g_j(x))_{j\in Z}$, we must prove that the intersection of Γ and V is reduced to one element. We as yet have no mathematical proof of this uniqueness; however, the numerical experiments described in Section VII show that the algorithm does reconstruct the wavelet transform of $f(x)$ for any initial sequence.

VI. Discrete Dyadic Wavelet Transform

A proper implementation of the zero-crossing representation and of the reconstruction algorithm raises several important questions. The input signal is generally measured with a finite resolution that imposes a finer scale when computing the wavelet transform. In practice, the scale parameter must also vary on a finite range. This section explains how to interpret mathematically a dyadic wavelet transform on a finite range of scales. In all previous sections, our model was based on functions of a continuous parameter x. We discretize the abscissa x and describe efficient algorithms for computing a discrete wavelet transform and its inverse. The results of the reconstruction algorithm from the zero-crossing representation is described in the next section.

In practice, we cannot compute the wavelet transform at all scales 2^j for j varying from $-\infty$ to $+\infty$. We are limited by a finite larger scale and a nonzero finer scale. Let us suppose for normalization purposes that the finer scale is equal to 1 and that 2^J is the largest scale. Let $f(x) \in L^2$. We first show that between the scales 1 and 2^J, the wavelet transform $(W_{2^j}f(x))_{1\le j\le J}$ can be interpreted as the details available when smoothing $f(x)$ at the scale 1 but which have disappeared when smoothing $f(x)$ at the larger scale 2^J. Let us introduce a function $\phi(x)$ whose Fourier transform is given by

$$|\hat{\phi}(\omega)|^2 = \sum_{j=1}^{+\infty} |\hat{\psi}(2^j\omega)|^2. \tag{25}$$

Since the wavelet $\psi(x)$ satisfies $\sum_{j=-\infty}^{+\infty} |\hat{\psi}(2^j\omega)|^2 = 1$, one can derive that $\lim_{\omega\to 0} |\hat{\phi}(\omega)| = 1$. The energy of the Fourier transform $\hat{\phi}(\omega)$ is concentrated in the low frequencies so $\phi(x)$ is a smoothing function. Let us define the smoothing operator S_{2^j} by

$$S_{2^j}f(x) = f * \phi_{2^j}(x),$$

with

$$\phi_{2^j} = \frac{1}{2^j}\phi\left(\frac{x}{2^j}\right). \tag{26}$$

The larger the scale 2^j, the more details of $f(x)$ are removed by the smoothing operator S_{2^j}. Let us prove that the dyadic wavelet transform $(W_{2^j}f(x))_{1\le j\le J}$ between the scales 1 and 2^J provide the details available in $S_1f(x)$ but not in $S_{2^J}f(x)$. The Fourier transform of $S_1f(x)$, $S_{2^J}f(x)$ and $W_{2^j}f(x)$ are respectively given by

$$\hat{S}_1f(\omega) = \hat{\phi}(\omega)\hat{f}(\omega), \qquad \hat{S}_{2^J}f(\omega) = \hat{\phi}(2^J\omega)\hat{f}(\omega), \tag{27}$$

and

$$\hat{W}_{2^j}f(\omega) = \hat{\psi}(2^j\omega)\hat{f}(\omega). \tag{28}$$

Equation (25) yields

$$|\hat{\phi}(\omega)|^2 = \sum_{j=1}^{J} |\hat{\psi}(2^j\omega)|^2 + |\hat{\phi}(2^J\omega)|^2. \tag{29}$$

Using Parseval's theorem, we derive from (27)–(29) the following energy conservation equation

$$\|S_1 f(x)\|^2 = \sum_{j=1}^{J} \|W_{2^j}f(x)\|^2 + \|S_{2^J}f(x)\|^2. \tag{30}$$

This equation proves that the higher frequencies of $S_1 f(x)$ that have disappeared in $S_{2^J}f(x)$ can be recovered from the dyadic wavelet transform $(W_{2^j}f(x))_{1\le j\le J}$ between the scales 1 and 2^J. The functions $S_{2^J}f(x)$, $(W_{2^j}f(x))_{1\le j\le J}\}$ are called the *finite-scale wavelet transform* of $S_1 f(x)$. In practice, the signal we process is given by a discrete sequence of values. The following lemma proves that any discrete signal of finite energy can be interpreted as the uniform sampling of some function smoothed at the scale 1.

Lemma 1: Let $D = (d_n)_{n\in Z}$ be a discrete signal of finite energy, $\sum_{n=-\infty}^{+\infty} |d_n|^2 < +\infty$. Let us suppose that for strictly positive constants C_1 and C_2 and all real ω, the Fourier transform $\hat{\phi}(\omega)$ satisfies

$$C_1 \le \sum_{n=-\infty}^{+\infty} |\hat{\phi}(\omega + 2n\pi)|^2 \le C_2.$$

There exists a (nonunique) function $f(x) \in L^2$ such that for any integer n

$$S_1 f(n) = d_n. \tag{31}$$

The proof of this lemma is in Appendix I. The discrete signal D can thus be rewritten $D = (S_1 f(n))_{n\in Z}$. For a particular class of wavelets $\psi(x)$ described in Appendix II, the samples $(S_1 f(n))_{n\in Z}$ enables us to compute a uniform sampling of the finite scale wavelet transform of $S_1 f(x)$

$$\{(S_{2^J}f(n))_{n\in Z}, ((W_{2^j}f(n))_{n\in Z})_{1\le j\le J}\}. \tag{32}$$

Let us denote

$$W_{2^j}^d f = (W_{2^j}f(n))_{n\in Z} \quad \text{and} \quad S_{2^j}^d f = (S_{2^j}f(n))_{n\in Z}. \tag{33}$$

The sequence of discrete signals $\{S_{2^J}^d f, (W_{2^j}^d f)_{1\le j\le J}\}$ is called a *discrete dyadic wavelet transform* of the signal $D = (S_1 f(n))_{n\in Z}$. If the signal D has N nonzero-samples, each discrete signal $W_{2^j}f$ has N nonzero samples so discrete dyadic wavelet transform has at most $N\log(N)$ nonzero samples. We denote by $\boldsymbol{W}^d$ the discrete wavelet transform operator that associates to a signal $\boldsymbol{D}$ the discrete wavelet transform previously defined. Appendix III describes a fast algorithm for implementing this operator. The complexity of this algorithm is $O(N\log(N))$. It is based on a cascade of convolutions with two discrete filters H and G. Appendix III also describes the implementation of the discrete inverse wavelet transform $\boldsymbol{W}^{-1,d}$ that reconstructs the signal $\boldsymbol{D}$ from its discrete dyadic wavelet transform. The reconstruction algorithm has also a complexity of $O(N\log(N))$. Fig. 4 is the graph of the wavelet that is used for all the numerical results shown in this article. The construction of this wavelet is described in Appendix II.

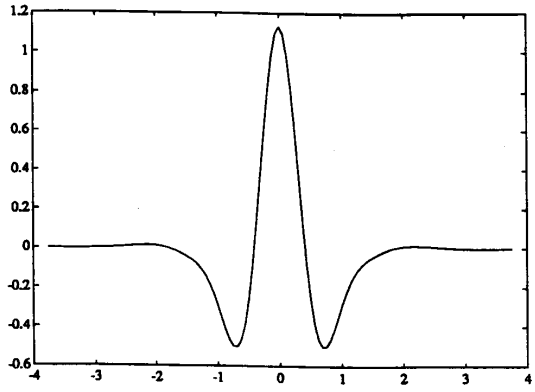

Fig. 4. Graph of the dyadic wavelet $\psi(x)$ used in the numerical experiments shown in this article. Wavelet is characterized numerically in Appendix II.

The zero-crossings of the functions $W_{2^j}f(x)$ are estimated from the sign changes of the samples of $W_{2^j}^d f$. The position of each zero-crossing is estimated with a linear interpolation between the two samples of different sign. The value of the integral e_n between two consecutive zero-crossings is estimated with the integral on the piecewise linear function that interpolates the samples of $W_{2^j}^d f$. If D has N nonzero samples, since there are at most $N\log(N)$ samples in the discrete wavelet representation, the number of operations to obtain the position of the zero-crossings as well as the integral values, is $O(N\log(N))$. From a discrete dyadic wavelet transform, we can only compute the zero-crossing positions and the integral values along the scales 2^j such that $1 < 2^j \le 2^J$. In order to keep the signal information at the scales larger than 2^J, we need to keep the coarse signal $S_{2^J}^d f$ in the zero-crossing representation. When J is large enough, this coarse signal is almost constant and equal to the average value of $f(x)$. We call *discrete zero-crossing representation* the set of signals

$$\{(Z_{2^j}f(x))_{1\le j\le J}, S_{2^J}^d f\}, \tag{34}$$

The signal in Fig. 5(a) is an image scan-line of 256 samples and Fig. 5(b) is its discrete wavelet transform computed with the wavelet shown in Fig. 4. The curves in both figures are linear interpolations between the samples of each discrete signal. The curve at the top of Fig. 5(b) is the coarse signal $S_{2^5}^d f$. Since the wavelet used is the second derivative of a smoothing function, the zero-crossings of the wavelet transform indicate the points of sharper variation at each scale. Fig. 5(c) shows the discrete zero-crossing representation obtained from the position of the

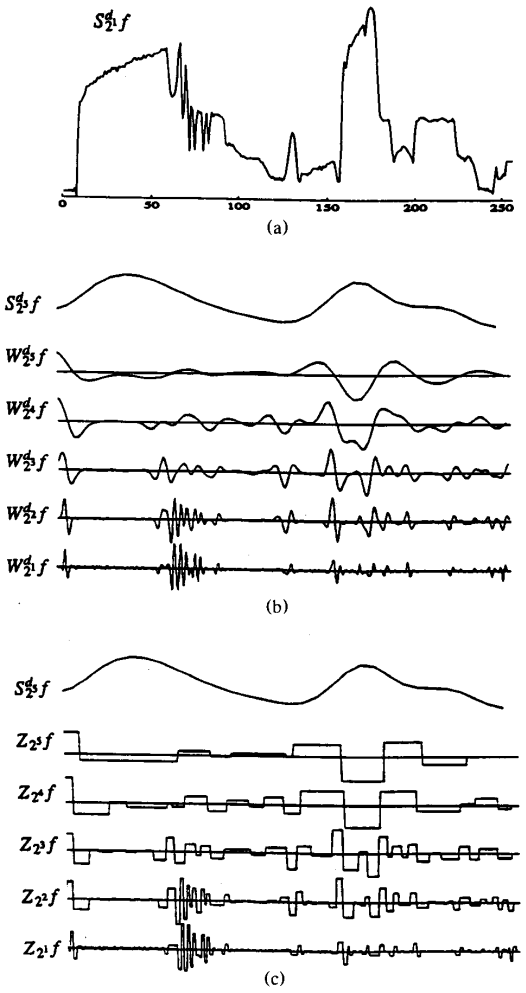

Fig. 5. (a) Image scan-line of 256 samples. (b) Dyadic wavelet transform of signal in Fig. 5(a) decomposed on 5 scales. Zero-crossings indicate the position of the sharp variation points. (c) Zero-crossing representation of signal in Fig. 5(a).

zero-crossings and the integral values estimated from each signal $W_{2^j}^d f$.

VII. Numerical Reconstruction from the Wavelet Transform Maxima

The algorithm that reconstructs the original signal from its local maxima representation, is based on two projection operators. The first one is the projection P_V on the space of all dyadic wavelet transforms. To any sequence of functions, it associates the dyadic wavelet transform of some function $f(x) \in L^2$. We saw in (12) that this operator can be decomposed into

$$P_V = W \circ W^{-1},$$

where W and W^{-1} are respectively the wavelet and inverse wavelet transform. Within a discrete framework, this operator is redefined by

$$P_V^d = W^d \circ W^{-1,d}, \tag{35}$$

where W^d and $W^{-1,d}$ are respectively the discrete wavelet transform and the inverse discrete wavelet transform. Since both W^d and $W^{-1,d}$ are implemented with fast algorithms of complexity $O(N \log(N))$, the numerical complexity for implementing P_V^d is also $O(N \log(N))$. The other projection operator involved in the reconstruction is the nonlinear projection on the set Γ. Appendix IV describes the discrete implementation of this operator that we denote P_Γ^d. The implementation of P_Γ^d has a complexity of $O(N \log^2(N))$. Let $P^d = P_\Gamma^d \circ P_V^d$. The reconstruction algorithm iterates on the operator P^d to reconstruct the intersection of V and Γ. We begin with an arbitrary initial sequence of discrete signals and iterate on the operator P^d until it converges to a fixed point. We apply the inverse wavelet transform operator $W^{-1,d}$ in order to compute the signal corresponding to the reconstructed dyadic wavelet transform.

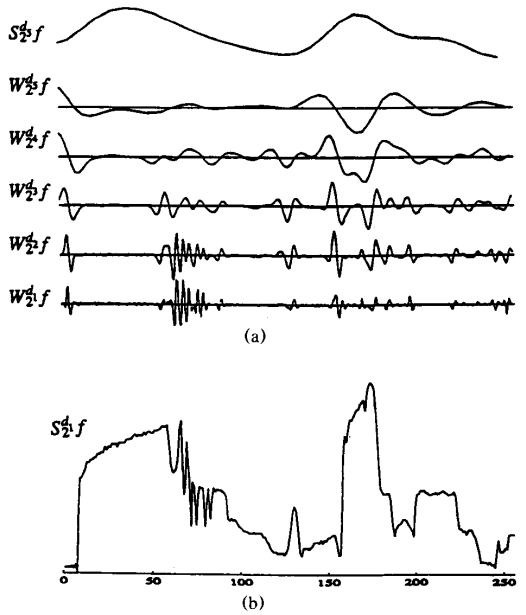

Fig. 6. (a) Reconstruction of the dyadic wavelet transform of the zero-crossing representation given in Fig. 5(c). This reconstruction was obtained with 15 iterations on the operator P^d. (b) Reconstruction of the signal by applying the inverse wavelet operator W^{-1} on the reconstructed wavelet transform of Fig. 6(a). Quality of the reconstruction can be appreciated by comparing this graph with Fig. 5(a).

Fig. 6(a) shows the reconstruction of the dyadic wavelet transform from the local zero-crossing representation given in Fig. 5(c), with 15 iterations on the projector P^d. Fig. 6(b) is the reconstruction of the original signal by applying the inverse wavelet transform operator on Fig. 6(a). The same quality of reconstruction was obtained for all the signals that we tested, including Diracs, step edges,

sinusoidal waves, Brownian processes, image scan-lines, etc. We observed that the reconstruction was independent from the initial sequence that we chose, which seems to indicate that the intersection of Γ and V is reduced to the wavelet transform of $f(x)$. This would mean that the zero-crossing representation is complete. The numerical stability of the iterative algorithm also indicates that the reconstruction is stable. We have tested the reconstruction from a zero-crossing representation with another wavelet that is much less regular. The same numerical results are obtained with this other wavelet. We therefore conjecture that for a large class of dyadic wavelets, the zero-crossings plus the integral values of $(W_{2^j}f(x))_{j\in Z}$ provide a complete and stable representation of $f(x)$. The class of wavelet for which this is true remains to be defined. We want to stress that this is only a conjecture based on numerical results, but no proof is given in the paper.

The performance of the reconstruction algorithm is particularly spectacular when $f(x)$ is a step edge. Indeed, we then only record the position of one zero-crossing at each scale and the value of the wavelet transform integral before and after this zero-crossing. This means that only three data values per scales are needed to reconstruct $f(x)$. In general, the amount of data in a zero-crossing representation depends upon the irregularity of the signal. For smooth signals with sparse singularities, this type of coding can be very compact.

VIII. Distance on a Zero-Crossing Representation

Pattern recognition is an important domain of application for such a zero-crossing representation. As explained in the introduction, the sharp variation points of a signal are often the most important features to identify patterns. This is the case in images where the discontinuities of the image intensity provide the contours of the important structures. The zero-crossings of a wavelet transform provide the location of the signal sharp variations. In order to compare two different zero-crossing representations for a pattern matching algorithm, it is necessary to define a distance. It is difficult to define such a distance just from the position of the zero-crossings but when the zero-crossing representation is stabilized with integral values, we can derive a natural mean-square distance.

The energy conservation (7) proves that the L^2 distance between two functions f and g can be expressed from their dyadic wavelet transform,

$$\|f(x)-g(x)\|^2=\sum_{j=-\infty}^{+\infty}\|W_{2^j}f-W_{2^j}g\|^2. \tag{36}$$

A simple estimate of this distance can be obtained from the zero-crossing representation $(Z_{2^j}f(x))_{j\in Z}$,

$$\boldsymbol{d}(\boldsymbol{Z}f,\boldsymbol{Z}g)^2=\sum_{j=-\infty}^{+\infty}\|Z_{2^j}f(x)-Z_{2^j}g(x)\|^2. \tag{37}$$

We prove in Appendix V that this distance is finite and satisfies

$$\boldsymbol{d}(\boldsymbol{Z}f,\boldsymbol{Z}g)^2\le\|f\|^2+\|g\|^2. \tag{38}$$

The distance $\boldsymbol{d}$ makes a global comparison of two zero-crossing representations over the entire spatial domain. A pattern is often a local feature embedded in the signal. For pattern matching purposes, we need to define a local distance which compares locally two zero-crossing representations. In order to derive such a distance from $\boldsymbol{d}$, we study the decomposition at all scales of a local feature such as a Dirac delta function $\delta_u(x)$ centered at u.

$$W_{2^j}\delta_u(x)=\delta_u(x)*\psi_{2^j}(x)=\psi_{2^j}(x-u). \tag{39}$$

Let 2σ be the size of an interval where the energy of $\psi(x)$ is mostly concentrated,

$$\int_{-\alpha}^{\alpha}|\psi(x)|^2\,dx\approx\int_{-\infty}^{+\infty}|\psi(x)|^2\,dx. \tag{40}$$

Equations (39) and (40) show that the energy of $W_{2^j}\delta_u(x)$ is mainly concentrated on the interval $[u-2^j\sigma,u+2^j\sigma]$. This interval defines the domain of influences of the point u, at the scale 2^j. In order to compare two zero-crossing representations $\boldsymbol{Z}f$ and $\boldsymbol{Z}g$ in the neighborhood of a point u, we define the local distance $\boldsymbol{d}_u$

$$\boldsymbol{d}_u(\boldsymbol{Z}f,\boldsymbol{Z}g)^2=\sum_{j=-\infty}^{+\infty}\boldsymbol{d}_u^j(Z_{2^j}f,Z_{2^j}g)^2, \tag{41}$$

with

$$\boldsymbol{d}_u^j(Z_{2^j}f,Z_{2^j}g)^2=\int_{u-2^j\sigma}^{u+2^j\sigma}|Z_{2^j}f(x)-Z_{2^j}g(x)|^2\,dx. \tag{42}$$

$\boldsymbol{d}_u^j(Z_{2^j}f,Z_{2^j}g)$ is a measure of the local distortion between $f(x)$ and $g(x)$ around the point u, at the scale 2^j. The integral of (42) is computed with few operations since the functions $Z_{2^j}f(x)$ and $Z_{2^j}g(x)$ are piece-wise constant. For a discrete zero-crossing representation, the local distance $\boldsymbol{d}_u$ is redefined with a finite sum as

$$\boldsymbol{d}_u(\boldsymbol{Z}f,\boldsymbol{Z}g)^2=\sum_{j=1}^{J}\boldsymbol{d}_u^j(Z_{2^j}f,Z_{2^j}g)^2. \tag{43}$$

IX. Application to Stereo-Matching

In order to illustrate the application of the zero-crossing representation to pattern matching, we study the implementation of a stereo-matching algorithm. Through this example, we intend to explain how to manipulate this representation for matching signals rather than developing a complete stereo system.

It is well known that one can recover the three dimensional coordinates of the surface that appear in a scene from a pair of stereo images. The main difficulty in this computation is to make a correspondence between the points that appear in the left image and the points in the right image. Let $\boldsymbol{P}$ be a point of the world that is projected on both images. Let P_l and P_r be respectively the projections of $\boldsymbol{P}$ on the left and the right images (see Fig. 7). One can compute the distance from $\boldsymbol{P}$ to the pair

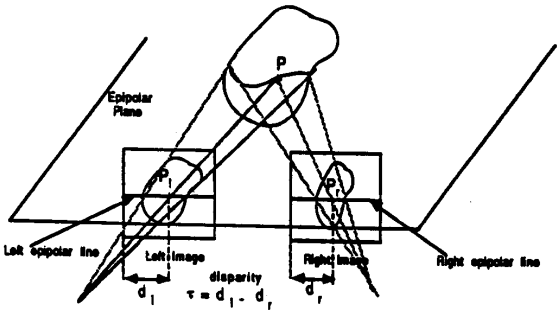

Fig. 7. Example of horizontal epipolar geometry of a pair of stereo images. Point P of the scene appears respectively in P_l and P_r in the left and right images, on the corresponding pair of epipolar lines. Disparity τ is the difference of positioning of P_l and P_r in each of the image. Disparity is inversely proportional to the distance between P and the pair of cameras.

of stereo cameras from the difference of positioning τ between P_l and P_r (see Fig. 7). This difference of positioning is called disparity. The goal of a stereo-matching algorithm is to find for each point P_l of the left image, the matching point P_r of the right image such that P_l and P_r are the projections of the same point P on the scene. The principle of such an algorithm is to look for a point P_r in the right image such that locally around P_r the image is the most similar to the neighborhood around P_l in the left image. Although this matching problem is *a priori* a two-dimensional search, it can be reduced to a one-dimensional search by using the epipolar geometry of the cameras. An epipolar plane is a plane that contains the point P and the optical centers of the left and right cameras. The intersections of such a plane with the left and the right images define a pair of epipolar lines. The stereo match of any point that is on a left epipolar line can be found on the corresponding right epipolar line. The problem is thus reduced to a one-dimensional matching problem along each pair of epipolar lines. Much research has been devoted to finding efficient algorithms for matching these epipolar lines [4], [15]. In particular Grimson has developed a coarse to fine matching algorithm based on multiscale zero-crossings. The principle of a coarse to fine strategy is to use first the information at large scales to perform the matching. Then the result of the matching are refined by progressively using the information at finer scales. A main difficulty of the Grimson algorithm is that we can not define a stable distance based on the zero-crossings only. In this section, we show that one can easily adapt the Grimson algorithm within a stablized zero-crossing representation and that the distance described in Section VIII enables us to implement a simple and efficient matching procedure.

Let us now explain in more detail how to match two epipolar lines from their zero-crossing representation. The epipolar line is a discrete one-dimensional signal. Let

$$\left\{(Z_{2^j}l(x))_{1\le j\le J}, S^d_{2^J}l\right\} \quad \text{and} \quad \left\{(Z_{2^j}r(x))_{1\le j\le J}, S^d_{2^J}r\right\}$$

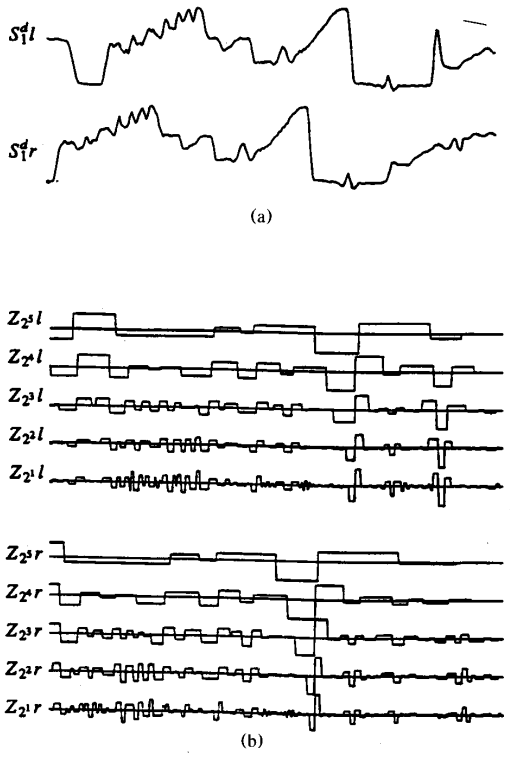

Fig. 8. (a) Pair of stereo epipolar scan lines from a real pair of stereo images. Distortion between these two signals is due to the difference of viewing perspective, to the camera noise and to the errors in the computation of the epipolar geometry. (b) Zero-crossing representations of the two epipolar lines. Top zero-crossing representation corresponds to the left signal and the bottom one to the right signal. We want to match these representations with a coarse to fine strategy.

be respectively the discrete zero-crossing representation of the left and right epipolar lines. Fig. 8(a) gives an example of pair of epipolar lines and Fig. 8(b) shows the corresponding zero-crossing representations. These epipolar lines were obtained from real images and as it can be observed, they are not only translated from one another but also distorted due to the perspectivity effect and the noise. We need to make a correspondence between the zero-crossings of both representations, at all the scales 2^j.

A coarse to fine strategy consists of matching first the coarser details of the two epipolar lines and then using the finer details to get more precise matches. Within the zero-crossing representation, we are first going to make the correspondence between the zero-crossings of $Z_{2^j}r(x)$ and $Z_{2^j}l(x)$ at the largest scale 2^j and then progressively decrease 2^j while using the information provided by the matches at the coarser scales in order to compute the matches at the finner scales. Given a zero-crossing z_n of $Z_{2^j}l(x)$ we want to find a zero-crossing $\tilde{z}_p$ of $Z_{2^j}r(x)$ such that if $\tau = z_n - \tilde{z}_p$ then $Z_{2^j}l(x)$ and $Z_{2^j}r(x-\tau)$ are as similar as possible in the neighborhood of $x = z_n$. Hence, the disparity τ is the value that minimizes the

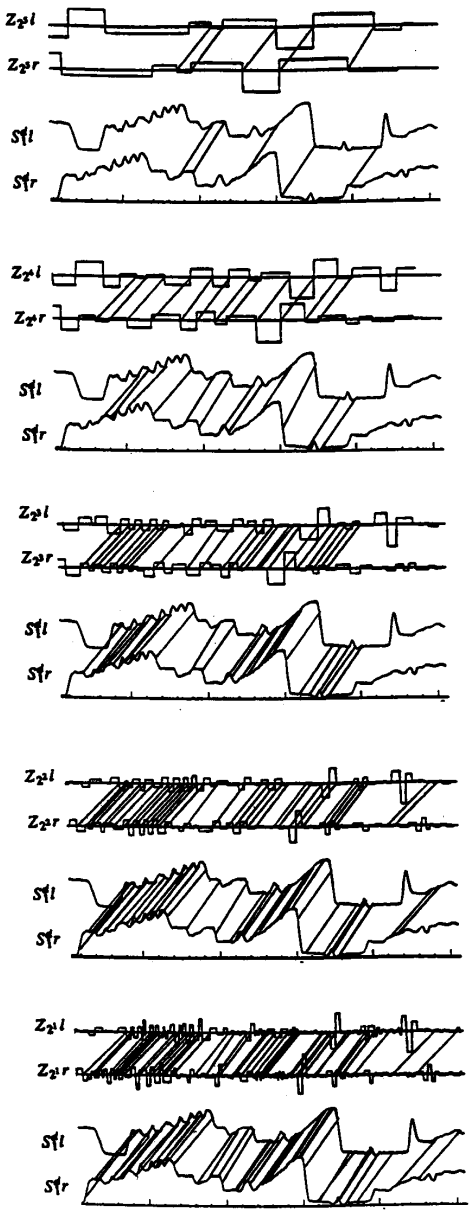

Fig. 9. Coarse to fine matching of the left and right zero-crossing representations. At each scale, we show at the top the zero-crossings that are matched and at the bottom the location of these matches on the left and right signals. When the scale decreases, there are more zero-crossings and hence more matches. However, not all zero-crossings can be matched at fine scales due to the high frequency distortions between the two epipolar lines.

local distance $d^j_{z_n}(Z_{2^j}l(x), Z_{2^j}r(x-\tau))$ defined in Section VIII. The minimum value $d_{\min}$ of the local distance gives also a confidence measure on the match. The smaller $d_{\min}$ the more similar the two functions $Z_{2^j}l(x)$ and $Z_{2^j}r(x-\tau)$ around $x = z_n$ and hence the higher our confidence in the match. Each match between a zero-crossing of $Z_{2^j}l(x)$ and a zero-crossing of $Z_{2^j}r(x)$ gives a local estimate of the disparity τ. At the next finner scale 2^{j-1}, we use this local estimate of the disparity in order to constrain the search when trying to find the correspondence between the zero-crossings of $Z_{2^{j-1}}l(x)$ and the zero-crossings of $Z_{2^{j-1}}r(x)$. When beginning at the coarser scale 2^J we do not have any prior estimation of the disparity to constraint the search. This is, however, not a problem since the number of zero-crossings of $Z_{2^J}l(x)$ and $Z_{2^J}r(x)$ is small when J is big enough (see Fig. 8(b)).

The coarse to fine strategy reduces considerably the complexity of the search for a match since we use the matching information at the previous scale to constrain the search at the next scale. This strategy supposes that we have a high confidence in the matches at the coarser scales since any error at a coarse scale might propagate at finer scales. The matching errors are due to the fact that the left and right signals are not only translated from one-another, but also distorted because of the noise and the perspectivity effect. Most of the distortion appears at the finer scales as shown in Fig. 8(b). We therefore have a better matching confidence at the coarse scales than at the finer scales.

In order to avoid side effects, at each scale, we did not try to match the zero-crossings at the boarders. As we can see from the successive matchings shown in Fig. 9, we are getting a dense matching on both signals. There are, some domains where we do not match the zero-crossings because there is too much distortion between $Z_{2^j}l(x)$ and $Z_{2^j}r(x)$. We have included in our algorithm a confidence threshold C in order to eliminate the matches where the minimal distance $d_{\min}$ is larger than $1/C$. Fig. 9 shows that in some domains, we find matches at a coarse scale but not at finer scales because there is too much high frequency noise.

The simple stereo matching algorithm can of course be enhance by using some further property of the disparity function such as a smoothness constraint [14] or a monotonicity constraint [4]. However, our goal here is more to illustrate the simplicity of the implementation of a matching algorithm with this zero-crossing representation, rather than develop a full stereo matching system.

X. Conclusion

We study the completeness, stability, and application to pattern recognition of a multiscale representation based on zero-crossings. The main result of the paper is an iterative algorithm that reconstructs the original signal from its zero-crossing representation. We proved the convergence of the algorithm but did not prove that the reconstruction is independent from the initial start of the iteration. The numerical experiments seem to indicate that the reconstruction is independent from the choice of the initial point which means that the zero-crossing representation is complete and stable. The proof of this result remains an open mathematical problem. In order to illustrate the application of this representation to pattern

matching, we described the implementation of a coarse to fine stereo-matching algorithm. The simplicity and the efficiency of this matching algorithm shows that this representation is indeed well adapted for pattern recognition problems.

In a zero-crossing representation, the number of values to be coded depends upon the irregularity of the signal. For signals that are mostly smooth with sparse singularities such as discontinuities, this type of coding can be very compact. In collaboration with Sifen Zhong, we have recently extended this representation in two dimensions [13], and shown that one reconstruct images from multiscale edges with a similar alternative projection algorithm. This image representation provides a compact reorganization of the information for a large class of images.

Appendix 1
Proof of Lemma 1

For any finite energy discrete signal $D=(d_n)_{n\in Z}$, we want to find $f(x)\in L^2$ such that

$$\forall n\in z, \qquad S_1 f(n)=d_n. \tag{44}$$

Let $f(x)\in L^2$, by definition we have $S_1 f(n)=f*\phi(n)$. This convolution product can be rewritten as an inner product in L^2: $S_1 f(n)=\langle f(x),\phi(n-x)\rangle$. Let U be the vector space generated by the family of functions $(\phi(n-x))_{n\in Z}$. If this family is a basis of U then for any discrete sequence $(d_n)_{n\in Z}$ of finite energy, there exists $f(x)\in L^2$ satisfying (44). One can show [10] than the family $(\phi(x-n))_{n\in Z}$ is a Hilbert basis if and only if for strictly positive constants C_1 and C_2, and all real ω, the Fourier transform $\hat{\phi}(\omega)$ satisfies

$$C_1\le \sum_{n=-\infty}^{+\infty} |\hat{\phi}(\omega+2n\pi)|^2\le C_2.$$

The values $(d_n)_{n\in Z}$ characterize the orthogonal projection of $f(x)\in L^2$ on U. This orthogonal projection can be interpreted as an approximation at the resolution 1 of the function $f(x)$ [11].

Appendix 2
A Particular Class of One-Dimensional Dyadic Wavelets

This appendix defines the class of wavelets used for implementation of discrete algorithms. From $(S_1 f(n))_{n\in Z}$ we want to be able to compute

$$\left\{(Z_{2^J} f(n))_{n\in Z},((W_{2^j} f(n))_{n\in Z})_{1\le j\le J}\right\},$$

with discrete convolutions. If $J=1$, this implies that we can compute $(S_{2^1} f(n))_{n\in Z}$ by convolving $(S_1 f(n))_{n\in Z}$ with a discrete filter H. In other words, the Fourier series of $(S_2 f(n))_{n\in Z}$ is equal to the Fourier series of $(S_1 f(n))_{n\in Z}$ multiplied by a 2π periodic function $H(\omega)$. The Fourier series of these two signals are respectively

$$\sum_{n=-\infty}^{+\infty} f*\phi(n)\,e^{-in\omega} \quad\text{and}\quad \sum_{n=-\infty}^{+\infty} f*\phi_2(n)\,e^{-in\omega}. \tag{45}$$

By applying the Poisson formula, we can rewrite these two series as

$$\sum_{n=-\infty}^{+\infty} \hat{f}(\omega+2n\pi)\hat{\phi}(\omega+2n\pi)$$

and

$$\sum_{n=-\infty}^{+\infty} \hat{f}(\omega+2n\pi)\hat{\phi}(2\omega+2n\pi). \tag{46}$$

The left series is equal to the right series multiplied by $H(\omega)$ for all $\hat{f}(\omega)$ if and only if

$$\hat{\phi}(2\omega)=H(\omega)\hat{\phi}(\omega). \tag{47}$$

Since $|\hat{\phi}(0)|=1$, we must have $|H(0)|=1$. If we cascade (47), we obtain a necessary condition on $\hat{\phi}(\omega)$,

$$\hat{\phi}(\omega)=\prod_{p=1}^{+\infty} H(2^{-p}\omega). \tag{48}$$

Conversely, if the 2π periodic function $H(\omega)$ satisfies

$$|H(\omega)|^2+|H(\omega+\pi)|^2\le 1, \tag{49}$$

then one can show [10] that the function $\phi(x)$ whose Fourier transform is defined by (49) is a function in L^2. The function $H(\omega)$ can be interpreted as the transfer function of a discrete low-pass filter.

Let us now characterize the corresponding wavelet $\psi(x)$. As a consequence of equation (29), we have

$$|\hat{\psi}(2\omega)|^2=|\hat{\phi}(\omega)|^2-|\hat{\phi}(2\omega)|^2. \tag{50}$$

Substituting (47) in (50) yields

$$\psi(2\omega)=G(\omega)\phi(\omega), \tag{51}$$

with

$$|G(\omega)|^2+|H(\omega)|^2=1. \tag{52}$$

The function $G(\omega)$ is chosen 2π periodic and can be interpreted as the transfer function of a high-pass filter.

For the zero-crossing model, we want to build a wavelet $\psi(x)$ equal to a second-order derivative of a smoothing function $\theta(x)$. This implies that $\hat{\psi}(\omega)$ must have a zero of order 2 in $\omega=0$. Since $|\hat{\phi}(0)|=1$, (51) yields that $G(\omega)$ must have a zero of order 2 in $\omega=0$. Table I gives the first coefficients of the impulse response of filters $H=(h_n)_{n\in Z}$ and $G=(g_n)_{n\in Z}$ that satisfy these properties. The impulse response of these filters is exponentially

TABLE I
First Five Coefficients of the Impulse Response of Filters H and G Corresponding to the Wavelet in Fig. 4

n	h_n	g_n
0	0.4347	0.7118
1	0.2864	−0.2309
2	0.0450	−0.1120
3	−0.0393	−0.0226
4	−0.0132	0.0062
5	0.0032	0.0039

decreasing and here we only give the first five coefficients. Both filters are symmetrical with respect to 0. The numerical experiments given in this paper are computed with these filters. For high precision computations, one needs to include more coefficients. The corresponding wavelet $\psi(x)$ is shown in Fig. 4. This wavelet has one small ripple on each side that can produce a few spurious zero-crossings. This ripple cannot be totally removed for the class of dyadic wavelet that we described in this appendix.

Appendix 3
Fast Wavelet Algorithms for One-Dimensional Signals

This appendix describes an algorithm for computing a discrete wavelet transform and the inverse algorithm that reconstructs the original signal from its wavelet transform. We suppose that the wavelet $\psi(x)$ is characterized by the two discrete filters $\boldsymbol{H}$ and $\boldsymbol{G}$ described in Appendix II. We denote H_p and G_p the discrete filters obtained by putting 2^p-1 zeros between each coefficients of the filters $\boldsymbol{H}$ and $\boldsymbol{G}$. The transfer function of these filters is respectively $H(2^p\omega)$ and $G(2^p\omega)$. We also denote by $\tilde{H}_p$ and $\tilde{G}_p$ the filters whose transfer functions are respectively $\overline{H(2^p\omega)}$ and $\overline{G(2^p\omega)}$ (complex conjugates of $H(2^p\omega)$ and $G(2^p\omega)$). We denote by $A * B$ the convolution of two discrete signals $\boldsymbol{A}$ and $\boldsymbol{B}$.

The following algorithm computes the discrete wavelet transform of the discrete signal $S_1^d f$. At each scale 2^j, it decomposes $S_{2^j}^d f$ into $S_{2^{j+1}}^d f$ and $W_{2^{j+1}}^d f$.

$j=0$,
WHILE $(j<J)$,
$W_{2^{j+1}}^d f = S_{2^j}^d f * G_j$,
$S_{2^{j+1}}^d f = S_{2^j}^d f * H_j$,
$j=j+1$,
END OF WHILE.

The proof of this algorithm is based on the properties of the wavelet $\psi(x)$ described in Appendix II. If the original signal $(S_1 f(n))_{n\in Z}$ has N nonzero samples, then each signal $S_{2^j}^d f$ and $W_{2^j}^d f$ has N nonzero samples. Since there are at most $\log(N)$ scales, the complexity of the algorithm is $O(N\log(N))$. The constant depends upon the number of nonzero coefficients in the filters H and G.

The inverse wavelet transform algorithm reconstructs $S_1^d f$ from the discrete dyadic wavelet transform. At each scale 2^j, it reconstructs $S_{2^{j-1}}^d f$ from $S_{2^j}^d f$ and $W_{2^j}^d f$. The complexity of this reconstruction algorithm is also $O(N\log(N))$.

$j=J$,
WHILE $(j>0)$,
$S_{2^{j-1}}^d f = W_{2^j}^d f * \tilde{G}_{j-1} + S_{2^j}^d f * \tilde{H}_{j-1}$,
$j=j-1$,
END OF FOR.

Appendix 4
Projection Operator on Γ

In this appendix, we describe more precisely the projection operators $\boldsymbol{P}_\Gamma$ defined in Section V. In order to define properly the set Γ, we first define the notion of zero-crossings for functions in $\boldsymbol{L}^2$. We shall say that a function $g(x)$ is strictly positive on an interval $[a,b]$ if

$$\forall (x,y)\in[a,b]^2, \qquad \int_x^y g(u)\,du \geq 0$$

and

$$\exists (x,y)\in[a,b]^2, \qquad \int_x^y g(u)\,du > 0. \tag{53}$$

The negative sign is defined by reversing the inequalities. A function $g(x)\in\boldsymbol{L}^2$ is said to have a zero-crossing in x_0 if there exists $\epsilon>0$ such that $g(x)$ is strictly positive (respectively negative) on the interval $[x_0-\epsilon, x_0]$ and strictly negative (respectively positive) on the interval $[x_0, x_0+\epsilon]$. Let us observe that if $f(x)$ is strictly positive on $[a,b]$, equal to zero on $[b,c]$ and strictly negative on $[c,d]$ then any point on the interval $[b,c]$ is a zero-crossing. In this case, we shall say that there exists only 1 zero-crossing, but this zero-crossing is unlocalized in the interval $[b,c]$. If a function $g_1(x)$ has one zero-crossing unlocalized in an interval $[b,c]$ and $g_2(x)$ has one zero-crossing in $x_0\in[b,c]$, we say that the position of the zero-crossing of $g_1(x)$ and $g_2(x)$ is the same. This definition is necessary in order to insure that the set Γ is closed.

Let us suppose that we record all the zero-crossings and integral values of the wavelet transform $(W_{2^j}f(x))_{j\in Z}$. The corresponding set Γ regroups all sequences of functions $(g_j(x))_{j\in Z}\in l^2(\boldsymbol{L}^2)$ such that $g_j(x)$ has the same zero-crossings and integral values than $W_{2^j}f(x)$ for all $j\in Z$. Given our definition of zero-crossing, one can prove without major difficulty that the set Γ is a closed convex in $l^2(\boldsymbol{L}^2)$.

Let us now define the operator $\boldsymbol{P}_\Gamma$ that transforms any sequence $(g_j(x))_{j\in Z}\in l^2(\boldsymbol{L}^2)$ into the closest sequence $(h_j(x))_{j\in Z}\in\Gamma$, with respect to the norm of $l^2(\boldsymbol{L}^2)$. Let $\epsilon_j(x)=h_j(x)-g_j(x)$. Each function $h_j(x)$ is chosen such that

$$\|\epsilon_j(x)\| = \int_{-\infty}^{+\infty}|\epsilon_j(x)|^2\,dx \text{ is minimum.} \tag{54}$$

Let z_{n-1} and z_n be respectively the abscissae of two consecutive zero-crossings of $W_{2^j}f(x)$ and e_n be the corresponding integral value. Let us suppose that $e_n>0$, the following conditions must be satisfied

$$\begin{cases} \displaystyle\int_{z_{n-1}}^{z_n} h_j(x)\,dx = \int_{z_{n-1}}^{z_n}\big(g_j(x)+\epsilon_j(x)\big)\,dx = e_n, \\ h_j(x) = g_j(x)+\epsilon_j(x)\geq 0, \qquad \text{for } x\in[z_{n-1}, z_n]. \end{cases} \tag{55}$$

The global minimization of $\|\epsilon_j(x)\|$ is equivalent to the

minimization of $\int_{z_{n-1}}^{z_n} |\epsilon_j(x)|^2\,dx$ for each pair of consecutive zero-crossings (z_{n-1}, z_n), with the two constraints

$$\begin{cases} \int_{z_{n-1}}^{z_n} \epsilon_j(x)\,dx = e_n - \int_{z_{n-1}}^{z_n} g_j(x)\,dx, \\ \epsilon_j(x) \geq -g_j(x), \quad \text{for } x \in [z_{n-1}, z_n]. \end{cases} \tag{56}$$

This minimization problem is solved by using the Lagrange multipliers. One can prove that there exists a lagrange multiplier λ such that

$$\epsilon_j(x) = \begin{cases} \lambda, & \text{if } -g_j(x) < \lambda, \\ -g_j(x), & \text{if } -g_j(x) \geq \lambda. \end{cases} \tag{57}$$

The value of λ is specified by the fact that

$$\int_{z_{n-1}}^{z_n} \epsilon_j(x)\,dx = e_n - \int_{z_{n-1}}^{z_n} g_j(x)\,dx. \tag{58}$$

Within a discrete model, Γ is defined as the set of all discrete signals $(g_j^d)_{j \in Z}$ such that each signal $g_j^d = (g_j(m))_{m \in Z}$ has the same zero-crossing position and integral values than the discrete signal $(W_{2^j} f(m))_{m \in Z}$. The set Γ is a closed convex. One can easily derive from our continuous model that the discretization of the nonexpansive projector on Γ consists in computing a discrete signal $\epsilon_j^d = (\epsilon_j(m))_{m \in Z}$ such that for any pair of consecutive zero-crossings (z_{n-1}, z_n) and integer $m \in [z_{n-1}, z_n]$,

$$\epsilon_j(m) = \begin{cases} \lambda, & \text{if } -g_j(m) < \lambda, \\ -g_j(m), & \text{if } -g_j(m) \geq \lambda, \end{cases} \tag{59}$$

and λ must be such that

$$\sum_{m \geq z_{n-1}}^{m < z_n} \epsilon_j(m) = e_n - \sum_{m \geq z_{n-1}}^{m < z_n} g_j(m) = c_n. \tag{60}$$

The most difficult to compute is the value of λ. Let K be the number of integers in the interval $[z_{n-1}, z_n[$. We first sort the values of $-g_j(m)$ for $m \in [z_{n-1}, z_n[$ so that $-g_j(m_K) \geq -g_j(m_{k-1}) \geq \cdots \geq -g_j(m_1)$. One can prove that λ is computed by the following algorithm.

$\lambda = \dfrac{c_n}{K}$,
$k = K$,
WHILE $(\lambda < -g_j(m_k))$
$\quad \lambda = \dfrac{k\lambda + g_j(m_k)}{k-1}$,
$\quad k = k - 1$,
END OF WHILE.

The total complexity for computing λ is $O(K \log(K))$ because of the first sorting step. To compute $\epsilon_j(m)$ once we know λ is done with (59) in $O(K)$ computations. If the original discrete signal $D = (S_1 f(m))_{m \in Z}$ has N nonzero samples, each signal g_j^d has also N samples so the computation of ϵ_j^d requires $O(N \log(N))$ operations. Since there are at most $\log(N)$ scales 2^j, the total number of computations to implement to discrete projector P_Γ^d is $O(N \log^2(N))$.

Appendix 5
Distance Between Zero-Crossing Representations

In this appendix, we prove that $\|Z_{2^j} f\| \leq \|W_{2^j} f\|$ and derive that

$$d(Zf, Zg)^2 \leq \|f\|^2 + \|g\|^2.$$

One can easily prove that among all functions that have an integral equal to a given value e on an interval $[a, b]$, the function which is constant on this interval has the minimum $L^2([a, b])$ norm. Between two consecutive zero-crossings z_{n-1} and z_n

$$\int_{z_{n-1}}^{z_n} Z_{2^j} f(x) = \int_{z_{n-1}}^{z_n} W_{2^j} f(x). \tag{61}$$

Since $Z_{2^j} f(x)$ is constant on the interval $[z_{n-1}, z_n[$,

$$\int_{z_{n-1}}^{z_n} |Z_{2^j} f(x)|^2 \leq \int_{z_{n-1}}^{z_n} |W_{2^j} f(x)|^2. \tag{62}$$

If there is a first zero-crossing z_0, we define $Z_{2^j} f(x)$ so that

$$\int_{-\infty}^{z_0} |Z_{2^j} f(x)|^2 \leq \int_{-\infty}^{z_0} |W_{2^j} f(x)|^2.$$

The equivalent is true if there is a last zero-crossing between this last zero-crossing and $+\infty$. We therefore derive that

$$\|Z_{2^j} f\|^2 = \int_{-\infty}^{+\infty} |Z_{2^j} f(x)|^2 \leq \int_{-\infty}^{+\infty} |W_{2^j} f(x)|^2 = \|W_{2^j} f\|^2. \tag{63}$$

Hence, we obtain

$$\sum_{j=-\infty}^{+\infty} \|Z_{2^j} f(x)\|^2 \leq \sum_{j=-\infty}^{+\infty} \|W_{2^j} f(x)\|^2 = \|f\|^2. \tag{64}$$

This proves that $(Z_{2^j} f(x))_{j \in Z} \in l^2(L^2)$. Since $d(Zf, Zg)^2 = \sum_{j=-\infty}^{+\infty} \|Z_{2^j} f(x) - Z_{2^j} g(x)\|^2$, (64) yields

$$d(Zf, Zg)^2 \leq \|f\|^2 + \|g\|^2.$$

References

[1] S. Curtis, S. Shitz, and V. Oppenheim, "Reconstruction of non-periodic two-dimensional signals from zero-crossings," *IEEE Trans. Acoust. Speech Signal Processing*, vol. 35, pp. 890–893, 1987.

[2] I. Daubechies, "The wavelet transform: A method of time-frequency localization," in *Advance in Spectral Analysis*, S. Haykin, Ed. New York: Prentice-Hall, 1990.

[3] ____, "The wavelet transform, time-frequency localization and signal analysis," *IEEE Trans. Inform. Theory*, vol. 36, no. 5, pp. 961–1005, Sept. 1990.

[4] W. Grimson, "Computational experiments with a feature based stereo algorithm," *IEEE Trans. Pattern Anal. Machine Intell.*, vol. 7, pp. 17–34, Jan. 1985.

[5] A. Grossmann and J. Morlet, "Decomposition of Hardy functions into square integrable wavelets of constant shape," *SIAM J. Math.*, vol. 15, pp. 723–736, 1984.

[6] R. Hummel and R. Moniot, "A network approach to reconstruction from zero-crossings," in *Proc. IEEE Workshop Computer Vision*, Dec. 1987.

[7] ____, "Reconstruction from zero-crossings in scale-space," *IEEE Trans. Acoust. Speech Signal Processing*, vol. 37, no. 12, Dec. 1989.

[8] J. Koenderink, "The structure of images," in *Biological Cybernetics*. New York: Springer-Verlag, 1984.

[9] B. Logan, "Information in the zero-crossings of band pass signals," *Bell Syst. Tech. J.*, vol. 56, p. 510, 1977.
[10] S. Mallat, "Multiresolution approximation and wavelet orthonormal bases of L2," *Trans. Amer. Mathematical Soc.*, vol. 315, pp. 69–87, Sept. 1989.
[11] ____, "A theory for multiresolution signal decomposition: The wavelet representation," *IEEE Trans. Pattern Anal. Machine Intell.*, vol. 11, no. 7, pp. 674–693, July 1989.
[12] ____, "Multifrequency channel decompositions of images and wavelet models," *IEEE Trans. Acoust. Speech Signal Processing*, vol. 37, no. 12, pp. 2091–2110, Dec. 1989.
[13] S. Mallat and S. Zhong, "Complete signal representation with multiscale edges," Comput. Sci. Tech. Rep. 483, New York Univ., Dec. 1989. To appear in *IEEE Trans. Pattern Anal. Machine Intell.*
[14] D. Marr and E. Hildreth, "Theory of edge detection," *Proc. Roy. Soc. Lon.*, vol. 207, 1980, pp. 187–217.
[15] D. Marr and T. Poggio, "A theory of human stereo vision," *Proc. Roy. Soc. Lon.*, vol. B204, 1979, pp. 301–328.
[16] Y. Meyer, in *Ondelettes et Operateurs*. Paris: Hermann, 1988.
[17] A. Rosenfeld and M. Thurston, "Edge and curve detection for visual scene analysis," *IEEE Trans. Comput.*, vol. C-20, pp. 562–569, 1971.
[18] J. Sanz and T. Huang, "Theorem and experiments on image reconstruction from zero-crossings," IBM, Res. Rep. RJ5460, Jan. 1987.
[19] M. J. Smith and T. P. Barnwell, "Exact reconstruction techniques for tree-structured subband coders," *IEEE Trans. Acoust. Speech Signal Processing*, vol. 34, June 1986.
[20] A. Witkin, "Scale space filtering," in *Proc. Int. Joint Conf. Artificial Intell.*, 1983.
[21] D. Youla and H. Webb, "Image restoration by the method of convex projections," *IEEE Trans. Med. Imaging*, vol. 1, pp. 81–101, Oct. 1982.
[22] A. Yuille and T. Poggio, "Scaling theorems for zero-crossings," *IEEE Trans. Pattern Anal. Machine Intell.*, vol. 8, Jan. 1986.
[23] Y. Zeevi and D. Rotem, "Image reconstruction from zero-crossings," *IEEE Acoust. Speech Signal Processing*, vol. 34, pp. 1269–1277, 1986.